IEEJ Journal of Industry Applications
Vol.7 No.4 pp.321–328 DOI: 10.1541/ieejjia.7.321

Paper

Investigating Iron Loss Properties in an Amorphous Ring Excited by Inverters based on Silicon and Gallium Nitride

Atsushi Yao[*,**a)] Member, Kouhei Tsukada[*] Non-member
Keisuke Fujisaki[*] Senior Member

(Manuscript received Oct. 16, 2017, revised Feb. 16, 2018)

In this study, we evaluate the iron losses in amorphous magnetic materials (AMM) and non-oriented (NO) rings excited by different inverters that use conventional and next-generation semiconductors. We examined the iron loss characteristics of the AMM ring as a function of carrier frequency when the ring was excited using two inverters. One inverter was a silicon-based insulated gate bipolar transistor (Si-IGBT) and the other was a gallium nitride-based field effect transistor (GaN-FET). We also compared the NO ring under these two inverter excitations. Due to the skin effect, the iron losses of the NO ring decreased with an increase in the carrier frequency under Si-IGBT inverter excitation. The AMM ring remained almost unaffected by the skin effect in the 1–20 kHz range; therefore, it is thought that the iron losses based on the AMM ring test fed by the Si-IGBT-inverter had an almost constant value. Under GaN-FET inverter excitation, the iron losses at high carrier frequencies increased because the number of times of ringing derived from the high-speed switching increased. We have shown that the influence of ringing in the AMM ring becomes large in comparison to that in the NO ring because the losses in the AMM ring are less than those in the NO ring in the high-frequency region.

Keywords: Iron loss, amorphous, non-oriented sheets, inverter, Si, GaN

1. Introduction

Pulse width modulation (PWM) inverters are often utilized to control the rotational torque and speed of an electrical motor in motor drive systems that have motor cores made of magnetic materials. In the recent times, many studies have shown that the iron losses in the magnetic core magnetized by PWM inverters increase due to the higher harmonic components superimposed in the current and voltage waveforms [(1)–(11)]. Some studies have focused on novel materials to reduce iron losses of the motor core, such as amorphous magnetic materials (AMM), which offer low iron losses in comparison with the conventional non-oriented (NO) silicon steel [(12)–(14)]. Therefore, it is important to understand the fundamental properties of iron loss with respect to the carrier frequency in the AMM core [(7)–(11)] under the PWM inverter excitation. This study aims to estimate the iron loss properties of the AMM core excited by PWM inverters with different semiconductors.

A power semiconductor is the main component of the inverter circuit. Recently, next-generation semiconductors such as silicon carbide (SiC) and gallium nitride (GaN) have been studied. These new materials for semiconductors are advantageous because they can be operated at high voltages and high temperatures; they have low on-resistance and fast switching. Recently, we have shown that the power semiconductor characteristics influence the magnetic hysteresis curves of NO materials [(2)]. In other words, there is some possibility that the iron loss in conventional NO materials changes by using PWM inverters with different power semiconductors. Therefore, the next phase is to correctly understand the influence of PWM inverters with conventional and next-generation semiconductors in AMM (the novel materials). Additionally, the understanding of the physical behavior is important to reduce the iron losses in the motor drive system.

This study focuses on the evaluation of iron losses of AMM excited by different PWM inverters using conventional and next-generation semiconductors. We examined the iron loss characteristics as a function of the carrier frequency of the AMM ring excited by two PWM inverters; one was a si-based insulated gate bipolar transistor (Si-IGBT) and the other was a gallium nitride-based field effect transistor (GaN-FET). We compared the NO ring under the two PWM inverter excitations to discuss the iron loss characteristics of the AMM. Additionally, to consider the physical behavior of iron loss properties in the NO and AMM rings, we addressed the skin effect and circuit model for the ringing noises generated by core and parasitic components. In particular, we focused on the convergence time of ringing (damped oscillations) in the AMM and NO rings.

a) Correspondence to: Atsushi Yao. E-mail: yao@pu-toyama.ac.jp
[*] Department of Advanced Science and Technology, Toyota Technological Institute
2-12-1, Hisakata, Tenpaku-ku, Nagoya 468-8511, Japan
[**] Department of Electrical and Computer Engineering, Toyama Prefectural University
5180, Kurokawa, Imizu 939-0398, Japan

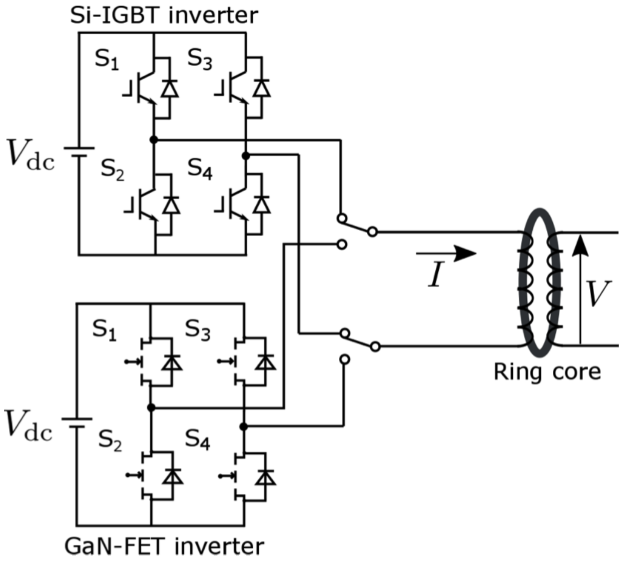

Fig. 1. Schematic of ring specimen and its measurement setup. The ring core is excited by either Si-IGBT or GaN-FET inverters

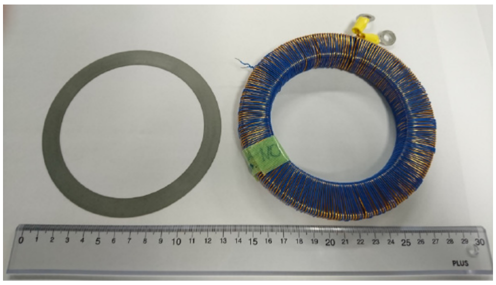

(a) NO ring

(b) AMM ring

Fig. 2. Ring specimens composed of laminations of NO sheets (35H300) and AMM (SA1). On the left side is the materials used for ring cores and on the right is the wound ring core. The two ring specimens have identical geometries

2. Ring Core and Its Measurement System

In this study, we examined the iron loss properties of ring specimens [6] made of NO sheets and AMM under a single phase PWM inverter. Figure 1 shows a schematic of the ring specimen and its measurement setup. This ring specimen was excited by two kinds of full bridge inverters. The first inverter was constructed using four GaN-FETs (DGF6010, Sanken Electric Corporation) and the second inverter consisted of four Si-IGBTs (PM75RSA060, Mitsubishi Electric Semiconductor). The on voltage of GaN-FET is low in comparison with that of Si-IGBT. We can realize the high-speed switching operation using the GaN-FETs.

Table 1. Specifications of materials used for the ring specimens

	NO	AMM
Reference	35H300	SA1
Density ϕ [kg/m^3]	7650	7180
Composition	Fe-Si	Fe-Si-B
Thickness [μm]	350	25
Saturation magnetic flux density [T]	2.12	1.56
Relative permeability μ_r	1550 Ref. (15)	5000 Ref. (16)
Resistivity ρ [$\mu\Omega$·m]	0.52 Ref. (17)	1.3 Ref. (18)
Iron loss at 50 Hz and 1 T [W/kg]	1.1	0.1

Table 2. Ring specifications

Characteristic	Symbol	Value
Height	h	7mm
Average magnetic path length	l	0.36 m
Cross section area	S	87.5 mm^2
Primary coil winding of AMM ring	N_1	254 turns
Secondary coil winding of AMM ring	N_2	254 turns
Primary coil winding of NO ring	N_1	252 turns
Secondary coil winding of NO ring	N_2	252 turns

Two ring specimens with identical geometries were manufactured, as shown in Fig. 2. The two ring specimens are composed of laminations of standard NO sheets (35H300) and AMM (SA1). The ring specimen made of AMM is impregnated with acrylic resin. Both ring laminations are cut using the wire cutting technique. The stacking factor of the AMM and NO cores is 0.91 and 0.99, respectively. In our rings, the inner diameter, the outer diameter, and the thickness of the rings were set to 102, 127, and 7 mm, respectively. Table 1 and Table 2 show the characteristics of materials (NO and AMM) used for the ring specimens and the ring specifications, respectively. This ring specimen has two coils wound with wire; the primary coil is used as the exciting coil and the secondary coil corresponds to a *B*-coil wound around the ring specimen to measure the magnetic flux density *B*.

We first need to obtain the magnetic field intensity (H) and magnetic flux density (B) to evaluate the iron loss properties of rings. In the experimental system, we measured the current (I) flowing in the primary coil of the ring specimen and the induced voltage (V) generated from the *B*-coil. From the measured I and V, the magnetic field intensity (H) and magnetic flux density (B) can be obtained as follows:

$$H = \frac{N_1 I}{l}, \quad \cdots\cdots (1)$$

$$B = \frac{1}{N_2 S} \int V dt, \quad \cdots\cdots (2)$$

where N_1 is the number of turns of the exciting coil, l is the magnetic path length, N_2 is the number of turns of *B*-coils, and S is the cross sectional area of the ring. Then, the iron losses of the ring specimen W can be calculated by integrating H and B as follows:

$$W = \frac{f_0}{\phi} \int H dB, \quad \cdots\cdots (3)$$

where ϕ is the density of the NO sheet or AMM. The current (I) and induced voltage (V) are measured by an analog to digital (A/D) converter (PXI-5122, National Instruments) that has a maximum sampling frequency of 100 MS/s realtime and a resolution of 14 bits.

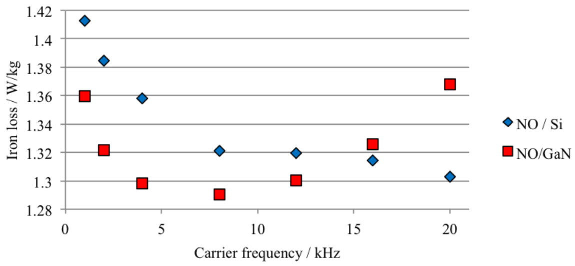

(a) NO Ring results

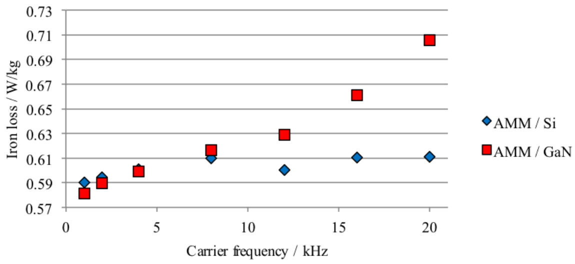

(b) AMM Ring results

Fig. 3. Experimentally obtained iron losses as a function of carrier frequency. Tests are done at magnetic flux density of 1.0 T. The blue (red) dots show iron losses under Si-IGBT (GaN-FET) inverter excitation

In the following experiments, the fundamental frequency (f_0), the modulation index, and the switching dead time were set to 50 Hz, 0.5, and 3500 ns, respectively. The maximum magnetic flux density (B_m) of the ring was adjusted by tuning the applied voltage and was set to 1.0 T. The ring tests were performed at carrier frequencies (f_c) of 1, 2, 4, 8, 12, 16, and 20 kHz.

3. Results and Discussion

In this section, we focus on the iron loss properties of the two rings excited by two PWM inverters. In addition, to discuss iron loss properties, we address the skin effect and the circuit model of the ringing noises generated by core and parasitic components. In particular, we focus on the convergence time of ringing in the AMM and NO rings.

3.1 Iron Loss and Hysteresis Properties Figure 3(a) shows the iron loss properties of the NO ring as a function of the carrier frequency under Si-IGBT and GaN-FET inverter excitations. The iron losses under Si-IGBT inverter excitation decrease with an increase in the carrier frequency. However, the iron losses of the GaN-FET inverter-excited NO ring decrease and then increase with increasing carrier frequency.

Figure 3(b) shows the iron loss properties of the AMM ring excited by inverters using Si-IGBT and GaN-FET with respect to the carrier frequency. The iron losses under Si-IGBT inverter excitation are almost constant. The AMM ring tests under GaN-FET inverter excitation at high carrier frequency show drastically large iron loss compared with that excited by the Si-IGBT inverter. As shown in Figs. 3(a) and 3(b), the iron losses of the rings for these four cases (NO and AMM rings under Si-IGBT and GaN-FET inverter excitations) have the different tendencies.

Figure 4 shows hysteresis loops of the NO ring excited by Si-IGBT and GaN-FET inverters. In Fig. 4, the graphs on the left are the magnifications of the minor loops in the NO ring. The height of the minor loop depends on the magnetic

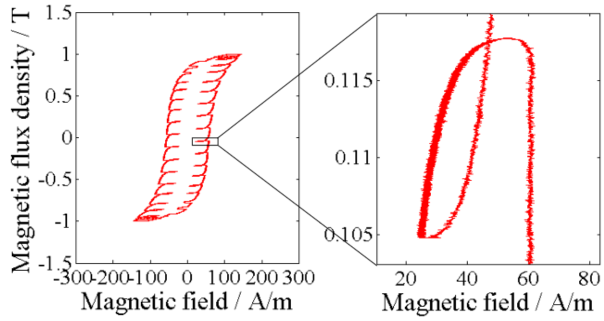

(a) $B-H$ loop at f_c = 1 kHz under Si-IGBT inverter excitation.

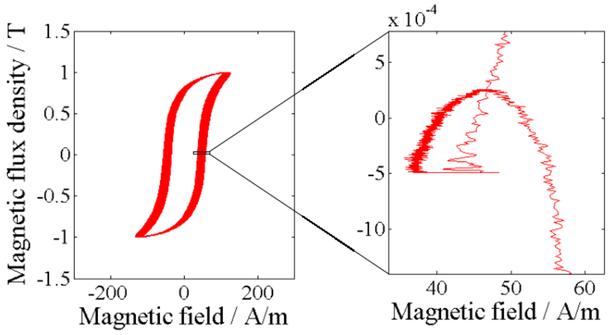

(b) $B-H$ loop at f_c = 20 kHz under Si-IGBT inverter excitation.

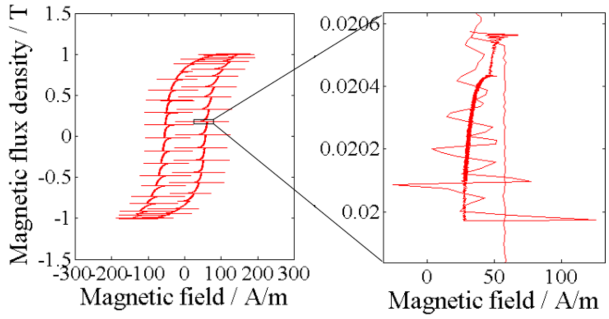

(c) $B-H$ loop at f_c = 1 kHz under GaN-FET inverter excitation.

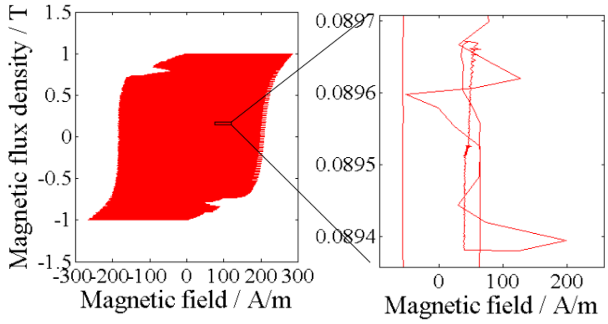

(d) $B-H$ loop at f_c = 20 kHz under GaN-FET inverter excitation.

Fig. 4. Hysteresis loops of the NO ring excited by Si-IGBT and GaN-FET inverters. The magnified figure shows the minor loop of the hysteresis loop

flux density of the Si-IGBT inverter shown in Fig. 4(a), which is larger than the magnetic flux density of the GaN-FET inverter shown in Fig. 4(c) because the on-voltage is low [2][4] for GaN-FET . See Appendix 1 for the details of the on-voltage of the induced voltage waveforms. The width of the minor loop related to H in the Si-IGBT inverter is much less than the width of the GaN-FET inverter. The high-speed switching generated ringing noises. Subsequently, the width of the minor loop became large in the GaN-FET inverter.

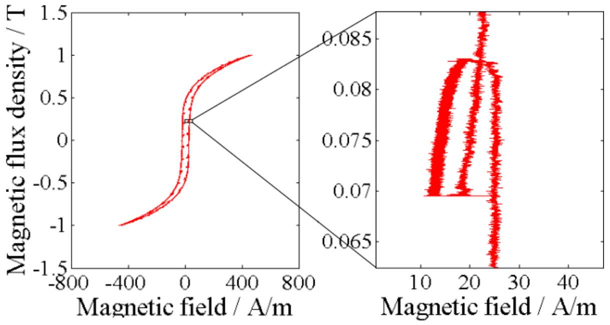

(a) Result at f_c = 1 kHz under Si-IGBT inverter excitation.

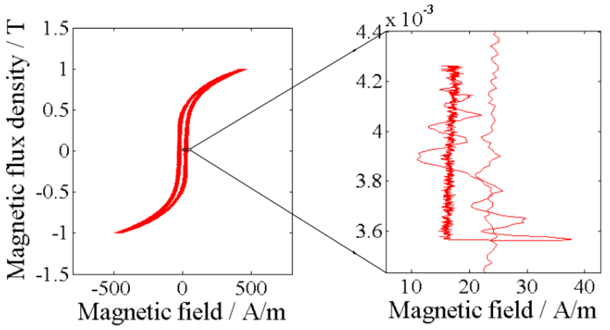

(b) Result at f_c = 20 kHz under Si-IGBT inverter excitation.

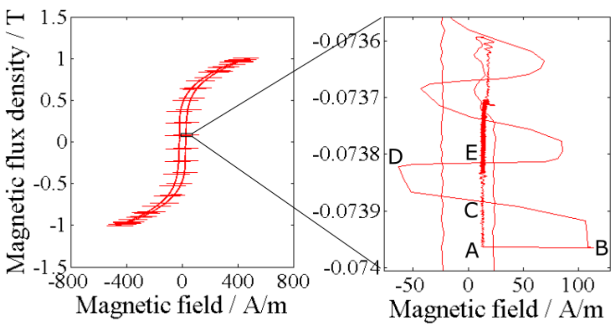

(c) $B-H$ loop at f_c = 1 kHz under GaN-FET inverter excitation.

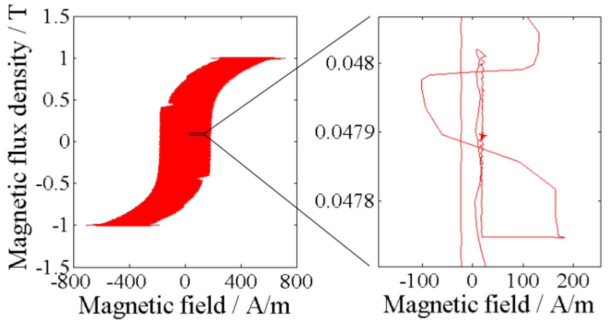

(d) $B-H$ loop at f_c = 20 kHz under GaN-FET inverter excitation.

Fig. 5. $B-H$ loops of the Si-IGBT- and GaN-FET-inverter-excited AMM ring. The magnified figure shows the minor loop, as in Fig. 4

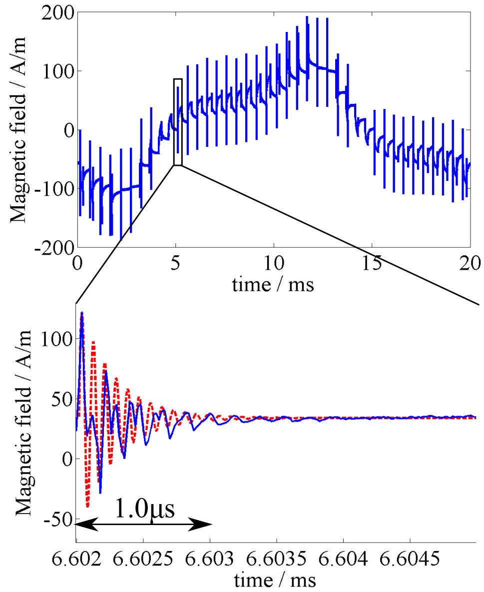

(a) Waveforms of the NO ring.

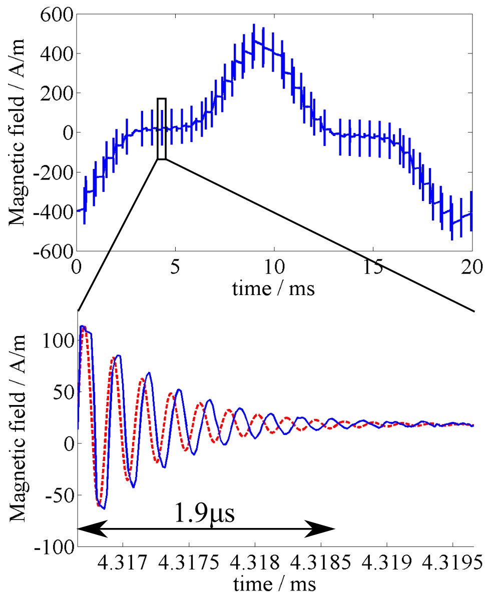

(b) Waveforms of the AMM ring.

Fig. 6. The waveforms of H in the NO and AMM rings under GaN-FET inverter excitation at f_c = 1 kHz. The magnified figure depicts the ringing generated by high-speed switching. In the magnified figure, the experimental waveform is the solid (blue) line and the corresponding waveform calculated by Eq. (7) is shown as the dashed (red) line

Figure 5 shows the $B-H$ curves of the AMM ring under Si-IGBT and GaN-FET inverter excitations. The minor loop of the AMM ring under Si-IGBT inverter excitation becomes small in comparison with that of the NO ring, as shown in Figs. 4(a) and 5(a). In the AMM ring under the GaN-FET inverter excitation shown in Figs. 5(c) and 5(d), ringing noises occurred in the magnetic field intensity, as well as in those in the NO ring. We found that the iron losses in the GaN-FET inverter-fed ring increased with increasing carrier frequency because the number of times of ringing increases, as shown in Figs. 4(c), 4(d), 5(c), and 5(d). For comparison purposes, see Appendix 2 for the details of iron loss and hysteretic properties under the six-step voltage excitation.

Figure 6 shows the waveforms of H in which ringing noises that are derived from high-speed switching occur. During the transient responses of the switching states in the GaN-FET inverter, ringing noises with large surge voltages generate current spikes and large changes of the field intensity due to core and the parasitic components present in the ring. Here the ringing waveform of H becomes asymmetrical. The area of the trace of A→B→C shown in the magnified figure in Fig. 5(c) is larger than the area of the trace of

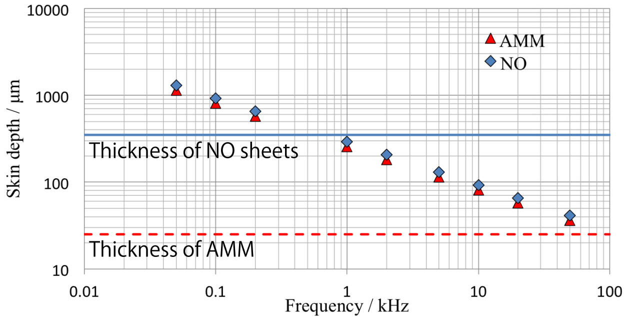

Fig. 7. Skin depth of NO (represented by blue dots) and AMM (represented by red dots). The solid (blue) and dashed (red) lines show the thickness of NO and AMM, respectively

C→D→E. Therefore, it is thought that iron losses increase because of ringing noises.

Figure 6(a) (6(b)) shows that it takes approximately 1.0 μs (1.9 μs) for the convergence of the ringing in the NO (AMM) ring. The convergence time in the AMM ring is longer than that in NO ring. Therefore, it is thought that, for iron losses, the influence of the ringing in the AMM ring becomes large in comparison with the ringing in the NO ring. Therefore, it is important to consider the effect of the ringing and its convergence time in the iron loss characterization. In the following section, we consider the reason for having different tendencies of iron loss properties for the four cases and for having a long convergence time for the ringing in the AMM ring based on the skin effect and the circuit model of the ringing generated by core and parasitic components.

3.2 Skin Effect We now discuss why the iron losses show different tendencies between the AMM and NO rings under different inverter excitations. It is well known that because of a remarkable skin effect, the eddy current loss of the magnetic material ring is mainly produced only near the surface of steel and the region that produces eddy current loss becomes small at a high carrier frequency. Thus, the iron losses in the magnetic material ring specimen decrease [19] when f_c becomes high [1]. Here, we consider the skin effect of the NO sheets and AMM. The approximation formula for the skin depth δ is usually given as

$$\delta = \sqrt{\frac{2\rho}{\omega\mu_0\mu_r}}, \cdots\cdots (4)$$

where ρ is the resistivity of the magnetic materials, ω is the frequency, μ_0 (= 1.26×10^{-6} H/m) is the permeability of the free space and μ_r is the relative permeability. Figure 7 shows the skin depth of AMM and the NO sheets. In the Fig. 7, the solid and dashed lines correspond to the thicknesses of the NO sheets and AMM. Within experimental parameters (1 kHz < f_c < 20 kHz), the iron loss properties of the NO ring under inverter excitation were affected by the skin effect, but the iron losses of the inverter-excited AMM ring were mostly not influenced by the skin effect. Therefore, under Si-IGBT inverter excitation, it is thought that the iron losses of the NO ring decrease with rising the carrier frequency because the region that produces the eddy current loss becomes small. The iron losses of the AMM ring under Si-IGBT inverter excitation have almost a constant value at 1 kHz < f_c < 20 kHz.

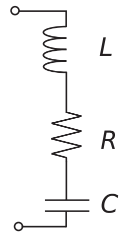

Fig. 8. *RLC* circuit model. Ringing phenomenon due to core and parasitic components is modeled by a series *RLC* circuit

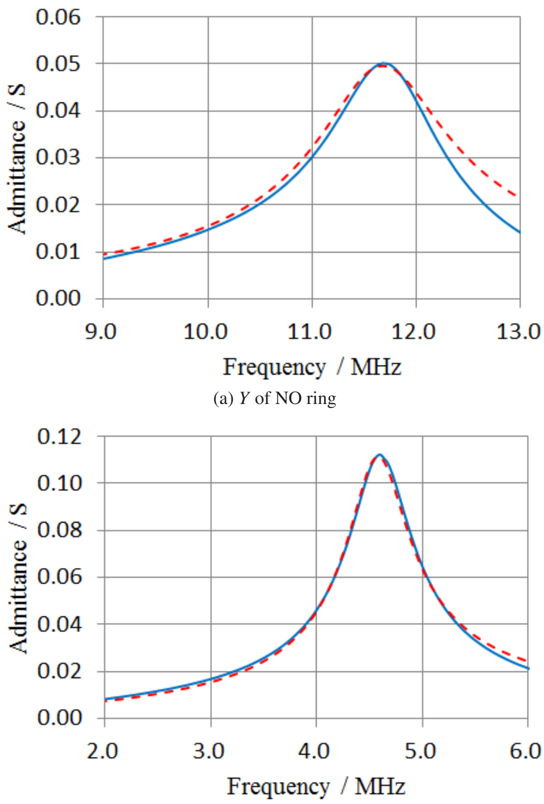

(a) *Y* of NO ring

(b) *Y* of AMM ring

Fig. 9. Admittance *Y* of AMM and NO rings. The solid (blue) line shows the experimentally obtained results by using an impedance analyzer (PSM3750, Iwatsu). The dashed (red) line are the fitted theoretical curves using Eq. (5)

3.3 Ringing Noises We discuss the convergence time of ringing (the damped oscillation) in the AMM and NO rings. We assume that the ringing phenomenon due to core and the parasitic components is modeled by a series *RLC* circuit consisting of a resistor *R*, an inductor *L*, and a capacitor *C*, as shown in Fig. 8. Here, it is thought that *C* depends on the parasitic capacitor. In the series *RLC* circuit, the admittance *Y* of the ring is given by

$$Y = 1/\left(R + j\left(\omega L - \frac{1}{\omega C}\right)\right). \cdots\cdots (5)$$

Figure 9 shows the experimentally obtained admittance *Y* of the AMM and NO rings. The admittance of the AMM and NO rings is measured by an impedance analyzer (PSM3750, Iwatsu). As shown in Fig. 9, the numerical frequency response curves are fit by Eq. (5) to the measured data (admittance). Thereby we obtained the numerically adjusted parameter as $R = 20.2\ \Omega$, $L = 2.68\,\mu$H, and $C = 69.4$ pF for NO ring and $R = 8.97\ \Omega$, $L = 2.56\,\mu$H, and $C = 472$ pF for AMM ring. Note that the resistor R depended strongly on the magnetic core materials used for the ring specimens. It is assumed that the ringing currents flow not only through the parasitic capacitor but also through the magnetic core. The R of the NO ring is larger than that of the AMM ring because the NO ring exhibits large losses in the high frequency region.

In the series *RLC* circuit, the differential equation and its damped oscillation ("ringing") are described by

$$L\frac{\mathrm{d}^2 i}{\mathrm{d}t^2} + R\frac{\mathrm{d}i}{\mathrm{d}t} + \frac{1}{C}\int i\mathrm{d}t, \qquad (6)$$

$$i(t) = A\mathrm{e}^{-\alpha t}\sin\beta t + B, \qquad (7)$$

$$\alpha = \frac{R}{2L}, \qquad (8)$$

$$\beta = \frac{1}{2L}\sqrt{R^2 - 4\frac{L}{C}}, \qquad (9)$$

where A and B are arbitrary constants. Here, α is the damping coefficient. By substituting the above fitting parameters for R, L, and C into Eq. (7), we can numerically obtain the ringing waveforms as shown by the dashed lines in the magnified figures in Fig. 6. The damped oscillation of the ringing (shown by the dashed red line shown in Fig. 6), which was calculated based on the series RLC circuit model, was well consistent with the experimental damped oscillation (shown by the solid blue line shown in Fig. 6). The value of α in the AMM ring (1.75×10^6 s^{-1}) is less than that in the NO ring (3.76×10^6 s^{-1}) because the losses in the AMM ring are lower than that in the NO ring in the high frequency region. Therefore, the convergence time of the ringing in the AMM ring becomes long in comparison with that of the NO ring. As shown in Fig. 6(a), a nonlinear damped oscillation is observed in the NO ring. In our future work, the ringing phenomenon with nonlinearity will be expressed by a new circuit model with nonlinear resistors. Additional numerical and experimental studies are necessary to investigate the inductor that depends on magnetic materials in the circuit model. In the near future, we will investigate the quantitative evaluation of the rate of increase of iron losses as a function of the ringing.

See Appendix 3 for the details of the current waveform of the ring specimen without magnetic material core. Here, as discussed in Appendix 3, it is assumed that C shown in Fig. 8 corresponds to the parasitic capacitor between the wire and magnetic material core. The details of the parasitic capacitors will be examined in our future studies.

In this study, we discussed the iron loss properties under certain conditions. Thus, we will propose to examine the reduction of the ringing currents under different conditions (*e.g.* by reducing the number of turns of the exciting coil).

Consequently, it is considered that the iron losses of the NO ring under the GaN-FET and Si-IGBT inverter excitation decreased because of the skin effect. The iron losses under the GaN-FET inverter excitation increased with increasing carrier frequency owing to the ringing noises. Additionally, the convergence time of the ringing in the AMM ring increased because the losses of the AMM ring were low compared with those in the NO ring in the high frequency region. Therefore, for the iron losses, the influence of the ringing in the AMM ring was large as compared with that in the NO ring. It is expected that the influence of these ringing noises appears in low loss magnetic materials that correspond not only to AMM but also to other novel materials such as nanocrystalline alloys (FT-3M [20]).

4. Conclusions

In this study, we examined the iron loss characteristics of AMM and NO rings under Si-IGBT and GaN-FET inverter excitations. We came to the following conclusions:

- The iron losses in the NO ring under Si-IGBT inverter excitation decreased with increasing carrier frequency since it is thought that the region, which produces eddy current loss, became small at high carrier frequency due to the skin effect.
- The AMM ring was almost unaffected by the skin effect ranging 1–20 kHz; therefore, the iron losses based on the Si-IGBT-inverter-fed AMM ring test were almost constant.
- Since the number of times of ringing derived from the high-speed switching increased, the iron losses at high carrier frequencies increased under GaN-FET inverter excitation.
- The AMM ring test under GaN-FET inverter excitation at high carrier frequency showed drastic large iron losses in comparison with the ring excited by Si-IGBT inverter.
- We found that the convergence time of the ringing in the AMM ring was greater than that in the NO ring.
- For iron losses, the influence of the ringing in the AMM ring was large as compared with the ringing in the NO ring.

Here, it is thought that, by using low loss materials (such as AMM) and next-generation semiconductors (such as GaN), the iron loss reduction in the motor drive system could not always be realized. In addition, it is expected that the influence of these ringing noises appears in low loss magnetic materials that correspond not only to AMM but also to other novel materials such as nanocrystalline alloys. Therefore, it is important to consider an optimized parameter setting of a system consisting of inverters and magnetic materials based on the understanding of their physical behavior. These results open the way for further research in iron loss reduction under different inverter excitations from the viewpoint of the entire system.

Acknowledgment

This work was partly supported by the JSPS KAKENHI ♯16H07320, the Ministry of Education, Culture, Sports, Science and Technology Program, Japan, for private universities, and Sanken Electric Corporation. We are grateful to Professor S. Odawara (Kitami Institute of Technology) for fruitful discussion.

References

(1) M. Kawabe, T. Nomiyama, A. Shiozaki, H. Kaihara, N. Takahashi, and M. Nakano: "Behavior of minor loop and iron loss under constant voltage type PWM inverter excitation", *IEEE Trans. on Magnetics*, Vol.48, No.11, pp.3458–3461 (2012)

(2) K. Fujisaki and S. Liu: "Magnetic hysteresis curve influenced by power-semiconductor characteristics in pulse-width-modulation inverter", *Journal of Applied Physics*, Vol.115, No.17, p.17A321 (2014)

(3) S. Odawara, K. Fujisaki, and F. Ikeda: "Proposing a numerical method for evaluating the effects of both magnetic properties and power semiconductor properties under inverter excitation", *IEEE Trans. on Magnetics*, Vol.50, No.11, pp.1–4 (2014)

(4) S. Odawara, D. Kayamori, and K. Fujisaki: "Iron loss characteristics of electrical steel sheet under inverter excitation by using power semiconductor with extremely low on-voltage property (in Japanese)", *IEEJ Trans. on Industry Applications*, Vol.134, No.7, pp.649–655 (2014)

(5) T. Taitoda, Y. Takahashi, and K. Fujiwara: "Iron loss estimation method for a general hysteresis loop with minor loops", *IEEE Trans. on Magnetics*, Vol.51, No.11, pp.1–4 (2015)

(6) A. Yao, K. Tsukada, S. Odawara, K. Fujisaki, Y. Shindo, N. Yoshikawa, and T. Yoshitake: "PWM inverter-excited iron loss characteristics of a reactor core", *AIP Advances*, Vol.7, No.5, p.056618 (2017)

(7) A. Boglietti, P. Ferraris, M. Lazzari, and M. Pastorelli: "Influence of modulation techniques on iron losses with single phase dc/ac converters", *IEEE Transactions on Magnetics*, Vol.32, No.5, pp.4884–4886 (1996)

(8) A. Boglietti, P. Ferraris, M. Lazzari, and F. Profumo: "Iron losses in magnetic materials with six-step and PWM inverter supply (induction motors)", *IEEE Transactions on Magnetics*, Vol.27, No.6, pp.5334–5336 (1991)

(9) A. Boglietti, P. Ferraris, M. Lazzari, and M. Pastorelli: "Change of the iron losses with the switching supply frequency in soft magnetic materials supplied by PWM inverter", *IEEE Transactions on Magnetics*, Vol.31, No.6, pp.4250–4252 (1995)

(10) W.A. Roshen: "Magnetic losses for non-sinusoidal waveforms found in ac motors", *IEEE Transactions on Power Electronics*, Vol.21, No.4, pp.1138–1141 (2006)

(11) W.A. Roshen: "A practical, accurate and very general core loss model for nonsinusoidal waveforms", *IEEE Trans. Power Electronics*, Vol.22, No.1, pp.30–40 (2007)

(12) H. Fujimori, H. Yoshimoto, T. Masumoto, and T. Mitera: "Anomalous eddy current loss and amorphous magnetic materials with low core loss", *Journal of Applied Physics*, Vol.52, No.3, pp.1893–1898 (1981)

(13) S. Okamoto, N. Denis, Y. Kato, M. Ieki, and K. Fujisaki: "Core loss reduction of an interior permanent-magnet synchronous motor using amorphous stator core", *IEEE Trans. on Industry Applications*, Vol.52, No.3, pp.2261–2268 (2016)

(14) N. Denis, Y. Kato, M. Ieki, and K. Fujisaki: "Core losses of an inverter-fed permanent magnet synchronous motor with an amorphous stator core under no-load", *AIP Advances*, Vol.6, No.5, p.055916 (2016)

(15) Non-oriented electrical steel sheets (in Japanese): Nippon Steel Corporation (2004)

(16) Nanocrystalline soft magnetic material (in Japanese): Hitachi Metals, Ltd., http://www.hitachi-metals.co.jp/products/elec/tel/pdf/hl-fm9-h.pdf

(17) Non-oriented electrical steel sheets (in Japanese): Nippon Steel and Sumitomo Metal Corporation, https://www.nssmc.com/product/catalog_download/pdf/D005je.pdf

(18) Amorphous alloy ribbon (in Japanese): Hitachi Metals, Ltd., http://www.hitachi-metals.co.jp/products/infr/en/pdf/hj-b10-b.pdf

(19) C. Kaido: "Method of evaluating anomalous eddy current loss in electrical steel sheets (in Japanese)", Journal of the Magnetics Society of Japan, Vol.33, No.2, pp.144–149 (2009)

(20) Y. Yoshizawa and K. Yamauchi: "Fe-based soft magnetic alloys composed of ultrafine grain structure", *Materials Transactions, JIM*, Vol.31, No.4, pp.307–314 (1990)

Appendix

1. Voltage Waveforms

app. Fig. 1 shows the induced voltage waveforms of NO ring under Si-IGBT and GaN-FET inverter excitations. Here, the input and induced voltage waveforms have almost the same value because the number of turns of the exciting and B-coils is the same. As shown in the magnified figures in app. Fig. 1, the on-voltage of GaN-FET is smaller than that of Si-IGBT because GaN-FET has low on-resistance. Therefore, the height of the minor loop in the GaN-FET inverter is smaller than that in the Si-IGBT inverter. See Refs. (2) and (4) for details of the relationship between the height of the minor loop and on-voltages.

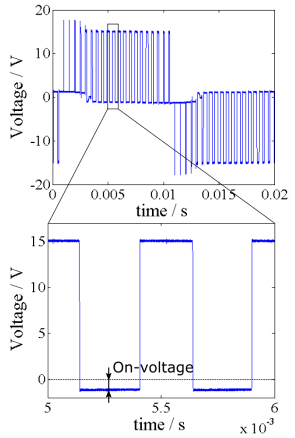

(a) Results at f_c = 1 kHz under Si-IGBT inverter excitation.

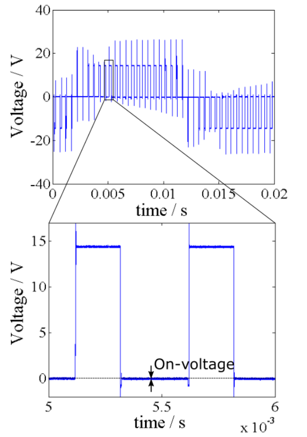

(b) Results at f_c = 1 kHz under GaN-FET inverter excitation.

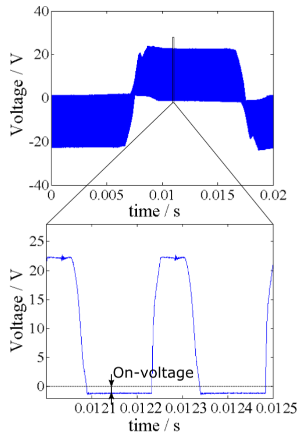

(c) Results at f_c = 20 kHz under Si-IGBT inverter excitation.

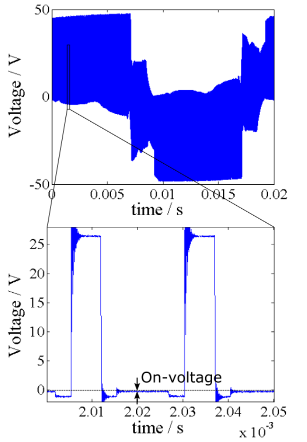

(d) Results at f_c = 20 kHz under GaN-FET inverter excitation.

app. Fig. 1. Induced voltage waveforms of NO ring under Si-IGBT and GaN-FET inverter excitations

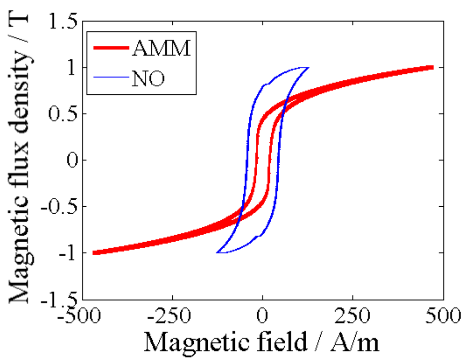

app. Fig. 2. Hysteresis loops of NO and AMM rings excited by six-step voltage

2. Iron Loss and Hysteretic Properties under Six-step Voltage Excitation

app. Fig. 2 shows hysteresis loops of NO and AMM rings excited by six-step voltage (rectangular waveform voltage). See Ref. (8) for details of six-step voltage. Here, the iron loss of NO (AMM) ring under six-step voltage excitation corresponds to about 1.13 (0.443) [W/kg]. Therefore, the iron loss of NO (AMM) ring at 1 kHz under Si-IGBT PWM inverter excitation is about 1.25 (1.33) times of that under six-step voltage excitation.

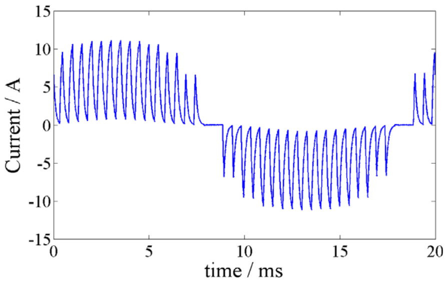

app. Fig. 3. Primary current waveform of the ring specimen without magnetic material core at f_c = 1 kHz under GaN-FET inverter excitation

3. Ring Specimen without Magnetic Material Core

app. Fig. 3 shows the primary current waveform, which is proportional to the magnetic field intensity, of the ring specimen without magnetic material core at f_c = 1 kHz under GaN-FET inverter excitation. Here, three rings (this ring specimen without magnetic material core, NO ring, and AMM ring) have identical geometries and identical coil winding. As shown in app. Fig. 3, there do not appear ringing noises in this ring specimen without magnetic material core. It is thought that when the magnetic material core exists, there appear ringing noises and then the parasitic capacitor. Here, it is assumed that C shown in Fig. 8 corresponds to the parasitic capacitor between the wire and magnetic material core.

Atsushi Yao (Member) received Ph.D. from Kyoto University in 2015. He was a postdoctoral researcher at Kyoto University and Toyota Technological Institute from 2015 to 2016 and 2016 to 2018, respectively. He is currently an assistant professor at Toyama Prefectural University. He is a member of IEEJ, JSAP, IEICE, and so on. His research interests are including applications and control of nonlinear dynamics in micro- and nano-system and power electronics.

Kouhei Tsukada (Non-member) received B.E. degree from Toyota Technological Institute in 2017. He is currently a master student at Toyota Technological Institute. His current scientific interests are power electronics.

Keisuke Fujisaki (Senior Member) received the B.Eng., M.Eng., and Dr.Eng. degrees in electronics engineering from the Faculty of Engineering, The University of Tokyo, Tokyo, Japan, in 1981, 1983, and 1986, respectively. From 1986 to 1991, he conducted research on electromagnetic force applications to steel-making plants at the Ohita Works, Nippon Steel Corporation. From 1991 to 2010, he was a chief researcher in the Technical Development Bureau, Nippon Steel Corporation, Futtsu, Japan. Since 2010, he was a professor of Toyota Technological Institute. His current scientific interests are magnetic multi-scale, electromagnetic multi-physics, high efficient motor drive system, electrical motor, and power electronics. In 2002–2003, he was a Visiting Professor at Ohita University. In 2003–2009, he was a Visiting Professor at Tohoku University. Dr. Fujisaki received the Outstanding Prize Paper Award at the Metal Industry Committee sessions of the 2002 IEEE Industry Applications Society Annual Meeting.